MAGNETIC RESONANCE
Open Access
Discussions

A CMOS-based NMR platform with arbitrary phase control and temperature compensation

Qing Yang[1], Jianyu Zhao[1], Frederik Dreyer[1], Daniel Krüger[1,2], Jens Anders[1,3]

[1] Institute of Smart Sensors, University of Stuttgart, Pfaffenwaldring 47, 70569 Stuttgart, Germany
5   [2] John A. Paulson School of Engineering and Applied Sciences, Harvard University, 29 Oxford Street, Cambridge, MA 02138, United States
[3] Center for Integrated Quantum Science and Technology (IQST)

Correspondence to: Jens Anders (jens.anders@iis.uni-stuttgart.de)

Abstract. In this paper, we present a custom-designed nuclear magnetic resonance (NMR) platform based on a broadband
10   complementary metal-oxide-semiconductor (CMOS) NMR-on-a-chip transceiver and a synchronous reference signal generator, which features arbitrary phase control of the TX pulse in combination with phase-coherent detection at a non-zero intermediate frequency (IF). Moreover, the presented direct digital synthesis (DDS) based frequency generator enables a digital temperature compensation scheme without the need for additional hardware. NMR spectroscopy and relaxometry measurements verify the functionality of the proposed frequency reference and temperature compensation scheme as well as the overall state-of-the-art
15   performance of the presented system.

1 Introduction

Nuclear magnetic resonance (NMR) is one of the most powerful analytical methods that allows for the direct measurement of molecular information. Due to its non-invasive nature and the possibility of measuring the NMR signal contactless, NMR is widely used in biomedicine (Peng et al., 2014; Chen et al., 2021), chemistry (Singh and Blumich, 2018), agriculture (Colnago et al., 2021)
20   and industrial applications (Rudszuck et al., 2021). Over the last ten to fifteen years, with technology advancements in the fields of magnet design, pulse sequences and electronics, NMR has seen two major areas of evolution: In high-field NMR, the increasing requirements for sensitivity and resolution lead to sophisticated and cumbersome NMR devices based on superconducting magnets with higher and higher magnetic field strength and very high filed homogeneity (Gan et al., 2017). These devices are capable of chemical structure analysis and medical imaging with unprecedented spectral and spatial resolution. In low-field NMR, the
25   development of chip-integrated CMOS-based NMR transceiver electronics (NMR-on-a-chip) (Sun et al., 2009; Ha et al., 2014; Grisi et al., 2015; Lei et al., 2016a; Handwerker et al., 2016; H. Bürkle et al., 2020) has led to portable NMR (pNMR) detection platforms based on permanent magnets, which are suitable for point-of-care applications (Lee et al., 2008; Liong et al., 2013; Ha et al., 2014; Lei et al., 2015; Lei et al., 2017; Lei et al., 2020).

As detailed in two recent review articles (Anders and Lips, 2019; Anders et al., 2021), the NMR-on-a-chip approach allows for
30   integrating the entire NMR console on a tiny footprint of a few square millimeters. To the best of our knowledge, the original idea of designing CMOS-based NMR electronics was presented by (Boero et al., 1998). Since then, the idea of integrating planar on-chip microcoils with CMOS transceivers has been widely employed (Lei et al., 2016b; Grisi et al., 2017; Handwerker et al., 2020) to produce miniaturized NMR detectors with very small detection volumes and very good spin sensitivities. Initially, the NMR-on-a-chip detectors were designed for operation inside conventional superconducting NMR magnets, focusing on the
35   miniaturization and parallelization of the NMR receiver (RX) (Boero et al., 2001; Anders and Chiaramonte, 2008; Kim et al., 2010; Anders et al., 2011). Later, with the advent of small-sized permanent NMR magnets, fully-integrated TX/RX NMR transceiver

MAGNETIC RESONANCE
Open Access Discussions

chips were developed to realize portable, low-field NMR detection platforms (Liu et al., 2008; Sun et al., 2011; Ha et al., 2014). The TX/RX transceivers were then also extended to high-field NMR by the use of on-chip wide-range frequency synthesizers (Kim et al., 2012; Grisi et al., 2015; Handwerker et al., 2016). More recent developments include improvements in the driving strength

40 of the NMR-on-a-chip transceivers by the use of high-voltage CMOS technologies (H. Bürkle et al., 2020; H. Bürkle et al., 2021) and the co-integration of electron spin resonance (EPR) electronics on a single chip to perform on-chip dynamic nuclear polarization (DNP) experiments (Solmaz et al., 2020). Very recently, Hong and Sun (2021) have presented an NMR-on-a-chip transceiver that allows for phase-synchronous detection at an arbitrary, non-zero intermediate frequency (IF) by using a dedicated design solution in the receiver path.

45 In this paper, we present a portable NMR system based on one of our NMR-on-a-chip transceiver application-specific integrated circuits (ASICs) with augmented functionalities. More specifically, the proposed NMR system provides the possibility of arbitrary phase modulation of the excitation pulse and phase-coherent detection of the resulting NMR signal at a non-zero IF by the use of two commercially available direct digital synthesizer (DDS) chips. Additionally, the presented system features an active temperature compensation based on the DDS frequency synthesizer (Issadore et al., 2011; Lei et al., 2017).

50 The paper is organized as follows. Section 2 discusses some key design considerations of portable, low-field NMR platforms and introduces the proposed system architecture. Section 3 then describes the utilized transceiver chip and DDS-based reference signal generator as well as the signal processing unit and the utilized probe head. Finally, section 4 provides measurements results of the proposed system that verify its functionality before the paper closes with a discussion and a brief outlook on future work in section 5.

55 2 Design consideration and system architecture

Before introducing the proposed system architecture, we will discuss some critical design considerations of portable NMR detection systems. In contrast to high-field NMR inside superconducting magnets, low-field NMR based on permanent magnets and NMR-on-a-chip transceivers suffers from a low signal-to-noise ratio (SNR) and magnetic field drift. The former is mainly due to the low polarization levels, the low operating frequency, and the limited transmitter power of NMR-on-a-chip transceivers. The

60 latter is due to the large temperature coefficient of standard permanent magnet materials (up to 1200 ppm/K for Neodymium magnets and 500 ppm/K for Samarium-cobalt magnets).

2.1 Phase control

According to the reciprocity principle, the SNR of the NMR signal in the time domain[1] can be written as (Hoult and Richards, 1976; Hoult, 2000)

65
$$\text{SNR}_t = \frac{\omega_0 B_u M_0 V_s}{\sqrt{4kT\Delta f R_{coil}}}$$

where ω_0 is the nuclear Larmor frequency ($\omega_0 = \gamma B_0$), B_u is the unitary magnetic field of the detection coil, $M_0 \propto \omega_0$ is the nuclear magnetization, V_s is the sample volume, R_{coil} is the AC coil resistance, which is proportional to the square root of the operating frequency due to the skin effect[2] (Minard and Wind, 2001). k is Boltzmann's constant, T is absolute temperature, and Δf is the considered detection bandwidth. Thus, SNR decreases rapidly as the work frequency decreases (SNR $\propto \omega_0^{7/4}$), which is

70 one of the main limitations of low-field NMR.

---

[1] Ignoring the inhomogeneity factor
[2] Without considering the proximity effect

One standard method to improve the SNR is to repeat the NMR experiments many times and average the individual results in the time-domain, introducing a strong tradeoff between signal quality (SNR) and measurement time. Importantly, for time-domain averaging to work properly, the initial phase has to be constant across all individual NMR time traces. Today, most modern NMR spectrometers make use of quadrature detection (Keeler, 2013), allowing for both a receiver local oscillator (LO) frequency that

75 equals the excitation frequency (homodyne detection) as well as an offset between the excitation and the receiver local oscillator frequencies (low-IF detection) (H. Bürkle et al., 2020; Issadore et al., 2011; Hong and Sun, 2021). The former benefits from the intrinsically constant output phase but introduces a tradeoff between excitation efficiency (on-resonance vs. off-resonance excitation) and 1/f noise (on-resonance excitation results in zero IF while off-resonance excitation produces an intrinsic non-zero IF). The latter allows for both on-resonance excitation and a non-zero IF to alleviate the influence of 1/f noise on the overall SNR.

80 However, the low-IF approach also comes at the expense of an uncertain receiver phase if no dedicated countermeasures are taken. Hong and Sun (2021) proposed using a custom-designed solution for the phase synchronization problem. Their solution is based on delaying the TX signal generated by the pulse controller until the phase of the TX signal is in phase with the LO signal in the receiver. This is achieved by the use of a phase alignment detector (a phase-frequency detector followed by an RC filter and an inverting Schmitt trigger), which delays the software TX signal from the pulse controller until the TX signal is in phase with the

85 receiver LO signal. While this scheme works well for pulse schemes with fixed inter-pulse delays such as the CPMG sequences presented in Hong and Sun (2021), it is not suitable for experiments that require variable, precisely definable time intervals between consecutive excitation pulses such as e. g., inversion recovery (IR) experiments. More specifically, the phase alignment circuit proposed in Hong and Sun (2021) introduces a non-constant delay T_{delay} between the software TX signal from the pulse controller and the actual TX pulse, which can be as large as $T_{delay} \leq 1/f_{IF}$, where $1/f_{IF}$ is the period corresponding to the utilized IF

90 frequency. As an example, the IF of $f_{IF} = 50$ kHz used in Hong and Sun (2021) introduces an uncertainty in the actual pulse occurrence of up to 20 μs. To avoid this problem, it has to be possible to synchronize the receiver LO signal to the TX waveform at will without introducing non-constant delays in the TX timing.

Moreover, the phase of the TX signal should also be adjustable at will to enlarge the range of possible pulse sequences, including e. g., phase cycling. Phase-cycling is a very useful capability for low-filed NMR-on-a-chip platforms because it mitigates the effect

95 of gain and phase mismatch between the in-phase and quadrature outputs of the on-chip and PCB-based electronics without the need for (expensive) calibration. Without proper countermeasures, the gain and phase mismatch cause an imperfect cancelation of the image frequency, distorting the NMR spectrum, cf. e. g., (J. Anders et al., 2010). Phase cycling is an effective method to remove these artifacts (Rahman et al., 2016), which requires arbitrary phase control of the TX phase, and, if a non-zero IF is used, measures to ensure a coherent phase of the receiver LO signal.

In this paper, we propose a solution for the abovementioned problem based on two commercially DDS chips that allows for an

100 arbitrary intermediate frequency, an arbitrary phase of the TX signal, and a phase-coherent receiver LO signal without compromising the pulse timing. The details of the proposed scheme are given in section 3.2.

2.2 Temperature drift

In most state-of-the-art low-field NMR platforms, permanent magnets are used due to their small size and low power consumption[3]

105 (Alnajjar et al., 2021; Yang et al., 2021). One limitation of such systems is that temperature fluctuations can cause severe frequency drifts if no countermeasures are taken. For instance, considering a free induction decay (FID) signal with a full width at half maximum (FWHM) of 100 Hz in the frequency domain measured with a 0.5 T Neodymium permanent magnet, the temperature

---

[3] The shim coils do require some power

would need to be kept constant with a precision of around 0.004 ℃ to avoid artifacts in the spectrum. Fortunately, various methods can be used to stabilize the NMR spectrum against environmental temperature fluctuations. For example, keeping the magnet in a

110 temperature-controlled box is the most common method (Yu et al., 2018). However, this approach requires the temperature control of a large volume and is, therefore, quite power-hungry. Active static magnetic field compensation or excitation frequency calibration is another effective method (Issadore et al., 2011; Lei et al., 2015; Lei et al., 2017). Alternatively, several signal processing techniques based on the measured NMR signal can be used to complement the abovementioned hardware measures to improve system robustness against temperature fluctuations further (Morris et al., 1997; Ha et al., 2014).

115 In this paper, we also propose a solution for eliminating the effect of magnet temperature drift on the measurement results that uses a digital control loop to adjust the excitation frequency automatically based on the measured IF. The details of the proposed method are also given in section 3.2.
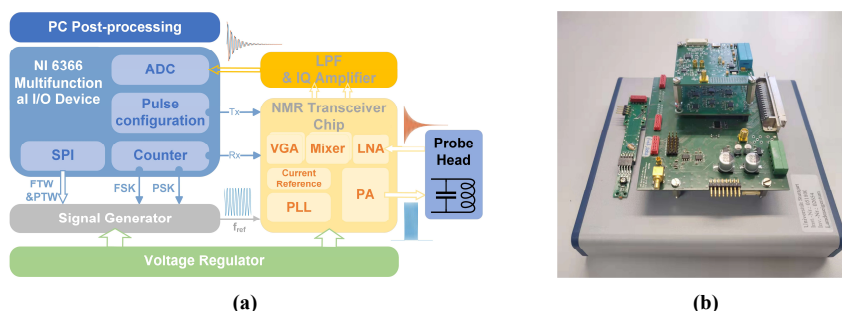
Figure 1. (a) Block diagram and (b) photograph of all electronics of the presented CMOS-based NMR platform

2.3 Proposed system architecture

120 The architecture of the proposed portable NMR system is shown in Fig.1. It comprises five main building blocks: i) an RF coil for sample excitation and detection of the NMR signal, ii) a CMOS NMR-on-a-chip transceiver containing all performance-critical analog transceivers electronics, iii) a reference signal generator to generate a frequency and phase adjustable TX and phase-synchronous receiver LO signal, iv) a digital signal processing unit for system control and signal acquisition, and v) a motherboard that integrates all required power management and further signal conditioning electronics such as anti-aliasing filters and level

125 shifters.

3 System implementation

3.1 NMR-on-a-chip transceiver and signal conditioning electronics

According to Fig. 2a, the custom-designed CMOS NMR-on-a-chip transceiver consists of a programmable integer-N phase-locked loop (PLL), a quadrature (IQ) generator, a power amplifier (PA), a low noise amplifier (LNA), a quadrature down-conversion

130 mixer and two variable gain amplifiers (VGAs). The PLL multiplies the external reference frequency by a selectable scaling factor between 0.5 and 64. The PLL can operate with reference frequencies between 5.7 MHz to 12.1 MHz, resulting in an output frequency operating range between 5.7 MHz and 770 MHz. The H-bridge-based PA uses a separate supply voltage of 2.5V and provides a maximum peak-to-peak output current of 180 mA into a 10 Ω load.

MAGNETIC
RESONANCE
Open Access
Discussions
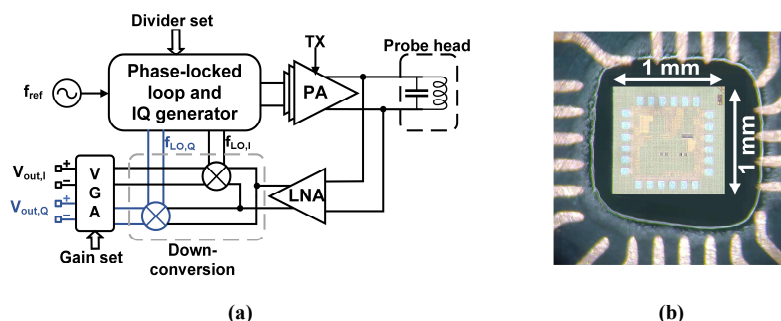
Figure 2. (a) Block diagram of the custom CMOS transceiver chip. (b) A micrograph of the chip attached to the PCB-based
135 **NMR-probe head.**

In the receiver path, the NMR signal is first amplified by an LNA and then down-converted by a quadrature mixer to an intermediate frequency (IF). Although zero-IF operation is possible, we typically operate the chip with an IF between 50 and 200 kHz to avoid SNR degradation due to flicker noise. The LNA features a state-of-the-art input-referred voltage noise of 770 pV/$\sqrt{Hz}$. The two digitally programmable VGAs provide a gain between 0 dB and 40 dB. The two VGAs are followed by a pair of off-chip, PCB-
140 based 4th-order Bessel low-pass filters (LPF) with a fixed gain of 14 dB and a fixed cutoff frequency at 350 kHz. The maximum overall gain of the RX chain is 99 dB. Figure 2b shows the micrograph of the NMR-on-a-chip transceiver. The chip is implemented in a 130 nm BiCMOS technology.

At this point, it is worth mentioning that the NMR-on-a-chip transceiver of Fig. 2a uses a single PLL with a single reference frequency to generate both the excitation signal and the local oscillator signal for the quadrature down-conversion mixer. In the
145 following section, we will explain how it is still possible to provide both excitation pulses with an arbitrary phase and timing and a phase-coherent down-converted NMR signal at a non-zero IF.

3.2 Proposed phase-coherent reference signal generator with temperature compensation

Direct digital synthesis (DDS) is a common choice for providing accurate reference signals in modern commercial NMR spectrometers because it can conveniently and rapidly change the frequency, phase, and amplitude of a waveform. To allow for
150 both phase coherence in the RX path and phase adjustability of the TX waveform, in this paper, we propose a synchronous reference signal generator based on two commercially available DDS chips AD9835 (Analog Devices), according to Fig. 3a. The two DDS chips (DDS1 and DDS2) utilize the same crystal oscillator (LFSPXO023414) with a clock frequency of 50 MHz to enable phase synchronicity between their two output signals. The 50 MHz reference frequency was selected to satisfy the Nyquist theorem with some margin for the largest NMR transceiver PLL reference frequency of 12.1 MHz. The AD9835 possesses two frequency
155 registers, each of which can be set by a 32-bit frequency tuning word (FTW). A one-bit frequency select input (FSELECT) then determines which FTW is used in the phase accumulator. Each AD9835 has two frequency registers that allow for fast switching between two different frequencies, e. g., to perform a frequency shift keying (FSK) modulation, where each frequency can be defined with a resolution of 11.6 mHz. Furthermore, there are four additional 12-bit phase tuning word (PTW) registers that allow for an arbitrary adjustment of the phase of the DDS output signal with a resolution of 1.53 mrad (0.088°). A two-bit phase select
160 input (PSEL0, PSEL1) determines which PTW is used for the phase accumulator. The output of each DDS chip is filtered and amplified by an active second-order Butterworth LPF with a cutoff frequency of 12.8 MHz and a gain of 6 dB. The current reference frequency for the CMOS transceiver, f_{ref}, is selected with an analog switch, TS5A63157 (Texas Instrument, Inc.), which displays a maximum delay of 5 ns and an isolation of -61 dB isolation.

(a)   **(b)**
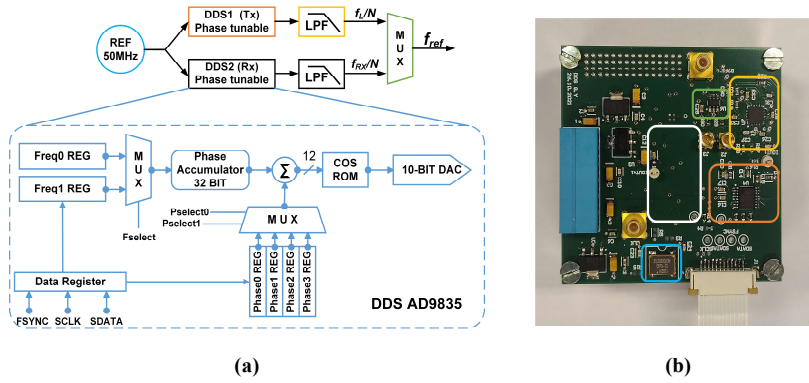
Figure 3. (a) Block diagram of the proposed DDS reference generator and (b) its PCB-based implementation on a 56×57
165 **mm two-layer PCB. Corresponding blocks are highlighted with the same color in the block diagram and the PCB photograph. The white rectangle indicates the position of the second DDS module on the bottom layer of the PCB.**

The detailed method to generate a reference frequency f_{ref} that allows for both an arbitrary adjustment of the TX phase and a phase-coherent receiver LO when operating at an arbitrary low-IF is as follows: first, the outputs of both DDS chips are deactivated, and their phase accumulators are set to zero. Then, two groups of FTWs are simultaneously loaded into the two frequency registers
170 of each DDS, the first corresponding to the Larmor frequency of the nucleus of interest f_L and the second to the desired receiver LO frequency ($f_{RX} = f_L + \Delta f$), respectively. Additionally, four PTWs ($0°, \frac{90°}{N}, \frac{180°}{N}, \frac{270°}{N}$), N being the divider ratio of the PLL of the CMOS transceiver chip, are also loaded into the four phase registers of each DDS. Here, it should be noted that the FTWs are initially selected such that both DDS chips start with the same output frequency of f_L/N[4]. Setting both DDS to a value of f_L/N ensures that the phase of the RX DDS is synchronous with the TX phase when the frequency of the NMR-on-a-chip transceiver is
175 changed to f_{RX}/N at the end of the TX pulse. We will explain this important point below in more detail. After that, both DDS outputs are activated. The digital control signal for the FSELECT port of DDS2 is triggered by the software TX signal. More specifically, a rising edge of the TX signal causes the output frequency of DDS2 to change from f_L/N to f_{RX}/N with a continuous phase. In this way, it is ensured that the receiver LO phase is synchronized to the phase of the latest excitation pulse, even when using different excitation pulse phases. Since the multiplexer switch is not toggled from DDS1 to DDS2 until the end of the TX
180 pulse, the PLL reference frequency f_{ref} remains connected to the output of DDS1, which still operates at a frequency of f_L/N, ensuring an excitation of the spin ensemble at a frequency of f_L. At the falling edge of the TX signal, the new reference frequency $f_{\mathrm{ref}} = f_{RX}/N$ is finally applied to the on-chip PLL, and the PLL locks to this new reference frequency and phase with a few microseconds[5]. Here, the on-chip PLL was designed to lock faster than the receiver's typical dead time. Overall, in this way, DDS1 is allowed to run continuously at a frequency of f_L/N, preserving its phase, which is the key requirement for phase-coherent
185 excitation pulses in multi-pulse NMR experiments, and DDS2 provides an LO signal for the NMR-on-a-chip transceiver that is coherent with the last excitation pulse. Figure 4a summarizes and illustrates the overall timing of the DDS output explained above for a single TX pulse. The PSEL bit can be used to select between different phases for the TX signal, i.e., the output of DDS1, to perform, e.g., phase cycling or generate a classical CPMG sequence. Figures 4b and c show how the PSEL is used to provide a

---

[4] Here it should be noted that although the reference frequency of the PLL corresponds to the excitation frequency, the transceiver chip is in the RX mode until the TX signal is set to high.
[5] The locking time is determined by the PLL bandwidth

MAGNETIC RESONANCE
Open Access Discussions

phase change of $\pm 90°$ in the output of DDS1. Finally, it should be noted that, for multi-scan measurements with averaging, the

190   phase accumulator must be set to zero after each scan.

In addition to providing a phase-coherent non-zero IF detection with arbitrary excitation phase, the presented DDS-based frequency synthesizer can also be used to solve the temperature drift problem explained in section 2.2. More specifically, to overcome this problem, our proposed NMR platform incorporates an automatic control loop, which automatically updates the FTW of each DDS to provide an on-resonance excitation at the Larmor frequency even in the presence of B_0 field drifts. The automatic control loop

195   works as follows: After each excitation pulse, the frequency information is extracted from the acquired FID or spin-echo signal, respectively. This measured frequency is compared with the predefined (in the control software) intermediate frequency of a selected peak in the spectrum. The implemented algorithm then updates the FTW of both DDS1 and DDS2 to provide an on-resonance excitation and keep the measured IF constant.

(a)

(b)

(c)
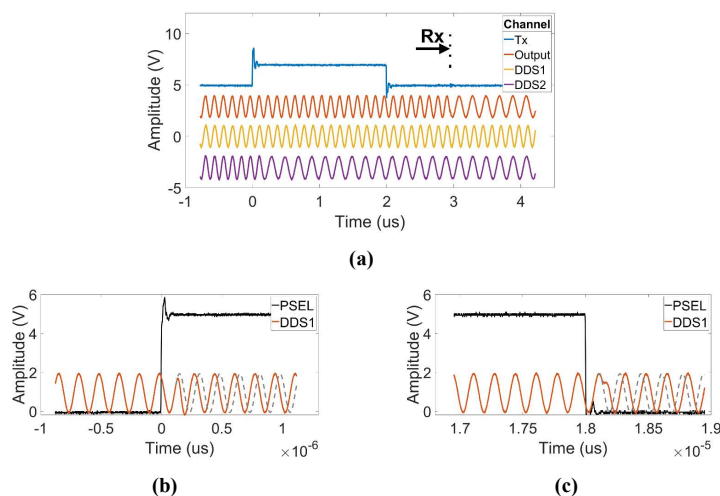
Figure 4. Illustration of the timing of the proposed DDS-based reference signal generator. (a) Frequency shift in the RX
200   **DDS at the rising edge of the TX pulse with a phase that is synchronous with the current TX phase. (b) and (c) Response to $\pm 90°$ phase shifts at the rising edge and falling edge of the PSEL digital signal.**

3.3 Data acquisition and digital signal processing

For data acquisition and digital signal processing, we used a commercial multifunction I/O device (USB-6366, National Instruments). The USB-6366 offers eight differential 16-bit analog input ports with a sampling rate of 2 MS/s/channel and 24

205   digital I/O channels. Our system uses an 8-bit digital output bus to generate the required digital control waveforms with a maximum sample frequency of 1 MHz, e.g., to communicate with the NMR-on-a-chip transceiver and the DDS chips via SPI. The USB-6366 also offers four 32-bit counters/timers, which can be used for pulse generation and event counting. To orchestrate the experiments, we have developed a custom-made Labview-based NMR control software. The software controls the communication with each DDS and the programmable NMR-on-a-chip transceiver, the generation of the NMR sequences, including phase control, and the

210   analysis of the acquired NMR signals.

3.4 NMR probe head

The NMR probe heads for the experimental results presented in this paper consist of the NMR coil and a tuning capacitor without matching to benefit from the intrinsic noise-free preamplification of the LC resonator formed by the coil and the tuning capacitor

MAGNETIC RESONANCE
Open Access Discussions

(Anders et al., 2016; Handwerker et al., 2013). Impedance matching is not required due to the close spatial proximity of the LC

215 resonator and the in-field NMR-on-a-chip transceiver.

To demonstrate the versatility of the proposed NMR platform, we have used two different solenoid coils with largely different sizes, cf. Fig. 5. The first coil (spectroscopy probe) is optimized for spin sensitivity. It is implemented as a 10-turn solenoidal coil by winding tightly – i.e., leaving a spacing as small as possible between adjacent turns – a 50 μm enameled copper wire around a small-diameter glass capillary (ID: 0.38 mm, OD: 0.4 mm). At 62 MHz, the coil displays a measured impedance of $(0.6 + j13.4)$

220 Ω with an inductance of 34.25 nH. In combination with our NMR-on-a-chip transceiver, the spectroscopy probe produces 90° pulse lengths of 5 μs, corresponding to an effective B_1-field of 1.2 mT. The second coil (relaxometry probe) was optimized towards improved concentration sensitivity for relaxometry measurements, taking into account the limited driving strength of the utilized broadband NMR-on-a-chip transceiver. It is implemented as a 10-turn solenoid by winding a 0.12 mm enameled copper wire around a larger glass tube (ID: 1.5 mm, OD: 2 mm) using the bifilar winding method (Wu et al., 1994). At 15.3 MHz, the coil

225 displays a measured impedance of $(1.0+ j15.0)$ Ω with an inductance of 156 nH. In combination with our NMR-on-a-chip transceiver, the relaxometry probe produces 90° and 180° pulse lengths of 18 μs and 38 μs, respectively. The latter value is deduced from the best echo quality. The 90° pulse length corresponds to an effective B_1-field of 330 μT.

Samples are inserted into the two coils by using capillary glass tubes with outer diameters of 0.3 mm and 1.3 mm, respectively.
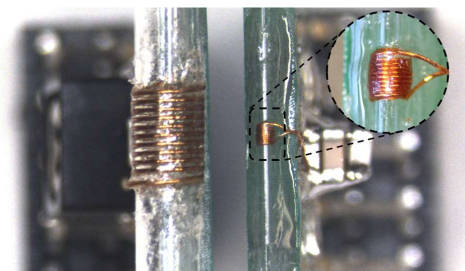
230 **Figure 5. Photograph of the two utilized NMR coils. Left: The relaxometry probe and right: the spectroscopy probe.**

For the following experiments, two types of magnets were used with B_0 field strengths of 0.36 T and 1.45 T. The first magnet $(B_0 = 0.36\,T)$, which we used for the relaxometry measurements, is a custom-designed system that features a small volume, a low weight, and a moderate homogeneity of 20 ppm. The second one $(B_0 = 1.45\,T)$, which we used for the spectroscopy experiments below, is a stripped-down Bruker MiniSpec magnet, which provides better homogeneity at a larger form factor and

235 weight.

4. Experimental results

In order to verify the performance of the proposed NMR platform, we have conducted a series of experiments. Here, we have first verified phase coherence between multiple acquisitions in multi-scan experiments for efficient time-domain averaging. To this end, we compared the phase distribution of the actual FID signals when using different reference signal sources for the NMR transceiver

240 chip. More specifically, a commercial waveform generator (Keysight 33600A) equipped with a frequency shift keying (FSK) option was used as an alternative reference signal source for our proposed DDS-based signal generator. The use of FSK for phase-coherent averaging in combination with NMR-on-a-chip transceivers and non-zero IFs was first proposed in Handwerker et al., (2020). This approach is sufficient for phase-coherent averaging in simple pulse-acquire experiments because all standard FSK implementations switch the frequency phase coherently (typically at the zero crossings of the phase). However, the FSK approach

245 does not allow for coherent control of the phase of the TX pulse across multiple pulses. In these experiments, we compared both on-resonance and off-resonance excitation. Here, off-resonance excitation allows for a non-zero IF without the need to switch the reference frequency between TX and RX at the expense of reduced excitation efficiency. We recorded ten consecutive FID signals for the commercial frequency generator and the proposed DDS-based solution using the relaxation probe filled with a vegetable oil sample and calculated the resulting phase distribution of the FIDs.

250 The detailed steps of calculating the phase distributions are as follows: The original FID signal length was first extended by a factor of three using zero padding. Then, we Fourier transformed the extended FIDs and adjusted the phase to obtain a pure absorption spectrum in the real part of the spectrum. Since there was only one line in the spectrum, it was sufficient to use a zero-order phase correction with a single correction phase[6] $\phi_{corr,i}$ (Keeler, 2013) for each FID. We then computed the mean and the standard deviation of the correction phases of all ten FIDs $\phi_{corr,i}$. The results are listed in Table I. The data clearly show that the

255 proposed DDS solution allows for phase-coherent time-domain averaging with a performance that is on par with a medium-prized commercial instrument.

Additionally, to test the system stability during a long-term averaging measurement, we also recorded one hundred consecutive FID signals. The average time-domain SNR for a single scan was 11.5. After averaging, the SNR was increased to 113, an enhancement of 9.8, which is very close to the theoretically predicted SNR improvement of $\sqrt{100} = 10$. Figure 6 shows the single

260 scan and time-averaged FID signals using the proposed DDS-based signal generator and an IF of 100 kHz.

Table I. Phase distribution of the recorded FID signals

|	Off-resonance (33600A)	On-resonance (33600A)	On-resonance (DDS)
Mean $\mu_{\phi_{corr,i}}$	13.09°	25.93°	-53.66°
Standard deviation $\sigma_{\phi_{corr,i}}$	0.27°	0.34°	0.17°
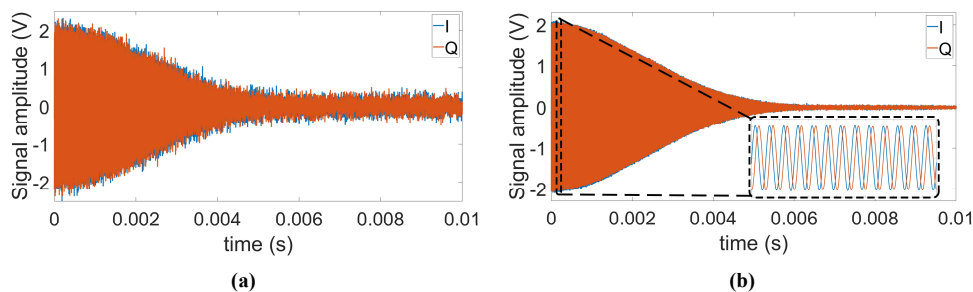
Figure 6. (a) Single scan and (b) time-averaged ($N_{scans} = 100$) FID signals using our proposed DDS-based reference signal generator.

265 Next, the FID of 21.2 nL pure ethanol sample was measured using the spectroscopy probe, cf. Fig. 7a. Figure 7b shows the real part of the corresponding Fourier spectrum. The position and amplitude of three peaks in the spectrum correspond to the expected chemical shifts and number of the hydrogen nuclei in the hydroxyl (OH), the methylene (CH2), and the methyl group (CH3).

---

[6] $\phi_{FID} = -\phi_{corr}$

Considering the time-domain SNR of the ethanol sample, the calculated time-domain spin sensitivity is 3.2×10^{16} spins/$\sqrt{\text{Hz}}$. (Anders et al., 2009)

**(a)**   **(b)**
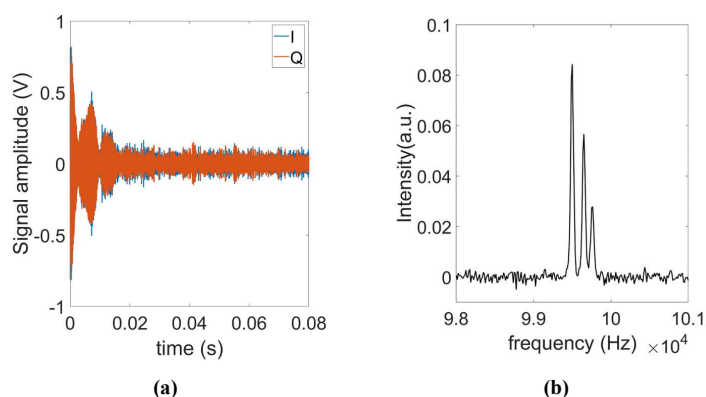
270   **Figure 7. (a) Single-shot FID of ethanol. (b) Real part of the corresponding Fourier spectrum.**

Having confirmed the functionality of the proposed scheme for coherent excitation and detection, we proceeded by measuring transverse relaxation (T_2) and longitudinal relaxation (T_1) times of sunflower oil, as an example of a homogeneous sample, with conventional CPMG and IR-FID sequences. The T_2 time was extracted with the following parameters for the CPMG sequence: number of echoes NE = 1000, echo time TE = 1 ms, and an echo duration of 0.6 ms. The T_1 time was extracted with the following

275   parameters for the IR-FID sequence: a minimum delay of 2 ms, a maximum delay of 702 ms, and a number of steps of 65. Here, the phase information of each FID (or echo using IR-echo sequence) can be used to distinguish the sign of those signals whose amplitudes are close to zero. Relying on a variable pulse delay between the first 180° pulse and the first 90° pulse, the IR sequence requires precise timing of said two pulses and a phase-coherent detection of the FID[7] or the echo[8]. Therefore, the IR experiments for T_1 extraction serve as an excellent benchmark application for the proposed DDS-based reference generators. Example data of

280   the CPMG and the IR measurements are shown in Fig. 8. The corresponding relaxation times derived from single exponential fitting were $T_2 = 84.9\ ms$ and $T_1 = 95.4\ ms$, respectively.

(a)   **(b)**
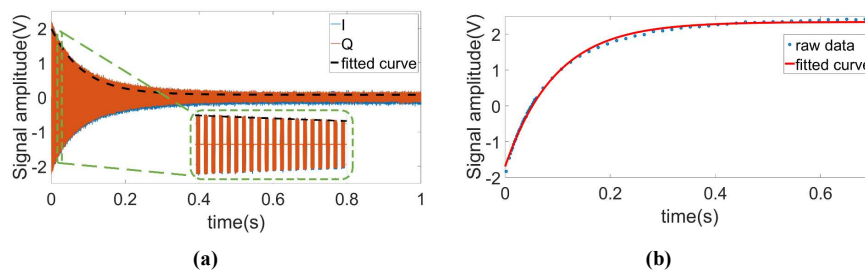
Figure 8. (a) CPMG signal and (b) IR signal of sunflower oil

Having verified the functionality of the proposed reference signal generator, we also tested the performance of the proposed temperature compensation scheme. Frequency shifts caused by temperature fluctuations not only reduce frequency-domain

285   resolution, cf. section 2.2, but also have a great influence on the accuracy of relaxation time measurements. More specifically, if

---

[7] For the IR-FID sequence
[8] For the IR-echo sequence

uncompensated, changes of the Larmor frequency over time lead to a drift of the excitation frequency away from said Larmor frequency. Therefore, the predefined pulse length is no longer correct, resulting in distorted CPMG signals. Here, two types of distortion are commonly encountered. The first one is an oscillation of the first few points of the CPMG signal, cf. Fig. 9a (left), and the second is an incomplete decay of the echo signal, cf. Fig. 9a (right). Figure 9b shows a series of CPMG experiments for a

290 continuous measurement of the transverse relaxation time (T_2) over a total experimental time of nearly 100 minutes without temperature control of the magnet. According to the figure, the Larmor frequency drifted over almost 5 kHz, but thanks to the frequency control loop, the T_2 time was still extracted with high accuracy. More specifically, the mean and standard deviation of all recorded T_2 values in Fig. 9b are 77.5 ms and 0.5 ms, respectively, corresponding to a normalized standard deviation of 0.65 %.


(a)   (b)
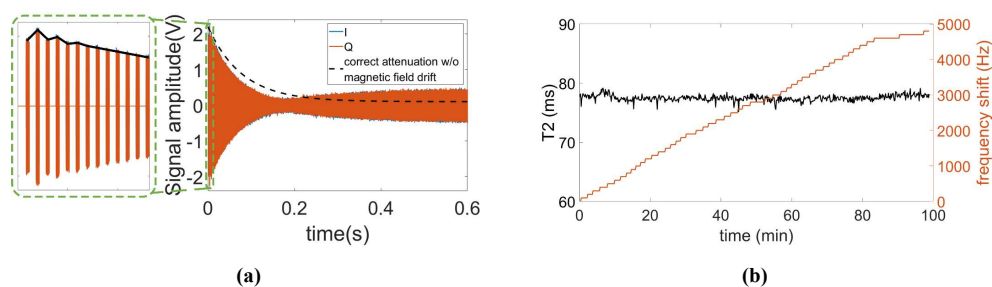
Figure 9. (a) Illustration of the effect of temperature-induced magnetic field drifts on the CPMG signal. (b) Continuously
295 **measured T_2 and the frequency drift of the magnet during the measurement time.**

To demonstrate that the presented platform is also capable of measuring the relaxation times of heterogeneous samples that contain material with different relaxation times, we have analyzed samples containing copper sulfate solutions with two different concentrations per sample with concentrations ranging from 5 mM/L to 75 mM/L. These samples were used to emulate bound, and unbound water samples since their distinction is a current application of NMR relaxometry (Stapf, 2010; Wu et al., 2021).

300 More specifically, we inserted the higher concentration sample into a 0.8 mm capillary, which was then inserted into a 1.3 mm capillary filled with a lower doped copper sulfate solution to construct a sample with two distinct relaxation times. Figure 10a shows an example time-domain CPMG signal of such a sample. From the time-domain data, we have extracted the relaxation times using double exponential fitting and cross-checked these results with the Inverse Laplace transform data, as shown in Fig. 10b, achieving an excellent matching between the two methods. The extracted T_2 and T_1 values are summarized in Table II. In these

305 experiments, the CPMG sequence parameters were: number of echoes NE = 2500, echo time TE = 0.4 ms, and an echo duration of 0.2 ms. The IR sequence parameters were: a minimum delay of 1 ms, a maximum delay of 801 ms (5 mM/L), 401 ms (10 mM/L), 201 ms (25 mM/L), or 81 ms ($\geq$ 50 mM/L), and a number of steps of 25.

Table II. Relaxation times of different concentrations of copper sulfate solution

Concentration (mM/L)	T_2 (ms)	T_1 (ms)
5	300.006 $\pm$ 1.817	332.467 $\pm$ 6.285
10	83.519 $\pm$ 1.056	93.178 $\pm$ 1.040
25	33.983 $\pm$ 0.729	41.69 $\pm$ 0.758
50	15.857 $\pm$ 0.297	17.85 $\pm$ 0.259
75	10.535 $\pm$ 0.101	13.918 $\pm$ 0.283
100	7.756 $\pm$ 0.111	9.768 $\pm$ 0.386

MAGNETIC RESONANCE Discussions

(a)

(b)
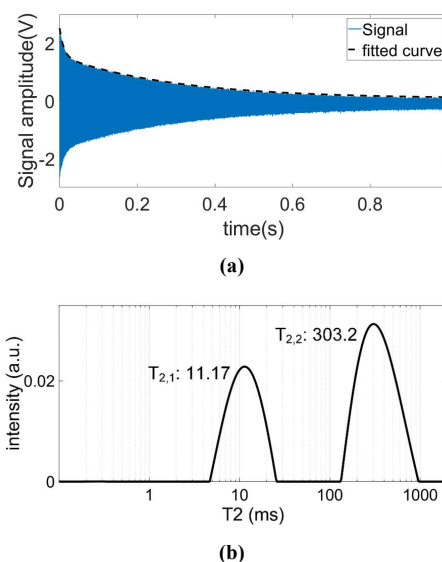
Figure 10. (a) An example time-domain CPMG signal of the constructed sample containing solutions with two different
310 **concentrations of copper sulfate doped water. (b) The corresponding T_2 distribution after inverse Laplace transform.**

5 Conclusion and discussion

In this paper, we have presented a CMOS-based NMR platform featuring arbitrary phase control and coherent detection in a non-zero IF receiver architecture as well as active automatic temperature compensation. The proposed platform is centered around a custom-designed NMR-on-a-chip transceiver. Thanks to the on-chip broadband PLL, our system can operate between 5.7 MHz
315 and 770 MHz. As one of the main innovations, the presented system features a DDS-based reference signal generator for the on-chip PLL that enables precisely timed excitation pulses with variable phase and - at the same time – phase-coherent detection at a non-zero IF. The proposed system achieves a phase stability well below 1° in consecutive pulse acquire experiments, which is on par with commercial equipment. NMR spectroscopy and relaxometry experiments inside 1.45 T and 0.36 T permanent magnets verified the versatility and excellent performance of the presented platform. Moreover, the proposed NMR platform includes an
320 automatic control loop that effectively counteracts frequency changes due to thermal drifts of the utilized permanent magnet. The efficiency of the frequency control loop is verified by T_2 measurements over 100 min, producing a normalized standard deviation in the measured T_2 values of 0.65 % in the presence of significant temperature fluctuations. The total peak power of all custom-designed electronics is 2.9 W, which allows for battery operation for several hours from a modern power bank. In the future, we will extend the presented platform NMR part by the possibility of performing Overhauser dynamic nuclear magnetization (ODNP)
325 using our EPR-on-a-chip transceivers for enhanced sensitivity in order to open up new application scenarios for portable NMR systems.

MAGNETIC RESONANCE
Open Access
Discussions

Code and data availability.

Code and data are available upon request.

330

Author contributions.

QY designed the reference signal generator and sequence generation program, designed the measurement setup and conducted measurements. JYZ designed the PCB board for the probe head and the transceiver chip and assisted with the measurements. FD and DK designed the transceiver chip. JA conceived the idea and experiments, designed the measurement setup. All authors

335   contributed to the manuscript.

Competing interests.

The authors declare that they have no competing interests.

Disclaimer.

Publisher's note: Copernicus Publications remains neutral with regard to jurisdictional claims in published maps and institutional

340   affiliations.

Acknowledgements.

Financial support.

References

Alnajjar, B. M. K., Buchau, A., Baumgartner, L., and Anders, J.: NMR magnets for portable applications using 3D printed materials, J Magn Reson, 326, 10.1016/j.jmr.2021.106934, 2021.

350 Anders, J. and Chiaramonte, G.: A Low-Noise CMOS Receiver Frontend for MRI, 2008 IEEE Biomedical Circuits and Systems Conference, 2008/11/20, 10.1109/BIOCAS.2008.4696900, 2008.

Anders, J. and Lips, K.: MR to go, J Magn Reson, 306, 118-123, 10.1016/j.jmr.2019.07.007, 2019.

Anders, J., SanGiorgio, P., and Boero, G.: A fully integrated IQ-receiver for NMR microscopy, J Magn Reson, 209, 1-7, 10.1016/j.jmr.2010.12.005, 2011.

355 Anders, J., Chiaramonte, G., SanGiorgio, P., and Boero, G.: A single-chip array of NMR receivers, J Magn Reson, 201, 239-249, https://doi.org/10.1016/j.jmr.2009.09.019, 2009.

Anders, J., Handwerker, J., Ortmanns, M., and Boero, G.: A low-power high-sensitivity single-chip receiver for NMR microscopy, J Magn Reson, 266, 41-50, 10.1016/j.jmr.2016.03.004, 2016.

Anders, J., Dreyer, F., Kruger, D., Schwartz, I., Plenio, M. B., and Jelezko, F.: Progress in miniaturization and low-field nuclear

360 magnetic resonance, J Magn Reson, 322, 106860, 10.1016/j.jmr.2020.106860, 2021.

Boero, G., de Raad Iseli, C., Besse, P. A., and Popovic, R. S.: An NMR magnetometer with planar microcoils and integrated electronics for signal detection and amplification, Sensors and Actuators a-Physical, 67, 18-23, 10.1016/S0924-4247(97)01722-6, 1998.

Boero, G., Frounchi, J., Furrer, B., Besse, P. A., and Popovic, R. S.: Fully integrated probe for proton nuclear magnetic resonance

365 magnetometry, Rev Sci Instrum, 72, 2764-2768, 10.1063/1.1374599, 2001.

Chen, Y., Jiang, X. W., Wang, J. N., Wu, Z. X., Wu, Y. C., Ni, Z. H., Yi, H., and Lu, R. S.: Sensitive Oxidation of Sorbitol-Mediated Fe2+ by H2O2: A Reliable TD-NMR Method for Clinical Blood Glucose Detection, Analytical Chemistry, 93, 14153-14160, 10.1021/acs.analchem.1c02616, 2021.

Colnago, L. A., Wiesman, Z., Pages, G., Musse, M., Monaretto, T., Windt, C. W., and Rondeau-Mouro, C.: Low field, time domain

370 NMR in the agriculture and agrifood sectors: An overview of applications in plants, foods and biofuels, J Magn Reson, 323, 10.1016/j.jmr.2020.106899, 2021.

AD9835: https://www.analog.com/en/products/ad9835.html#product-overview, last access: Feb 11 2011.

Gan, Z. H., Hung, I., Wang, X. L., Paulino, J., Wu, G., Litvak, I. M., Gor'kov, P. L., Brey, W. W., Lendi, P., Schiano, J. L., Bird, M. D., Dixon, L. R., Toth, J., Boebinger, G. S., and Cross, T. A.: NMR spectroscopy up to 35.2 T using a series-connected hybrid

375 magnet, J Magn Reson, 284, 125-136, 10.1016/j.jmr.2017.08.007, 2017.

Grisi, M., Gualco, G., and Boero, G.: A broadband single-chip transceiver for multi-nuclear NMR probes, Rev Sci Instrum, 86, 8, 10.1063/1.4916206, 2015.

Grisi, M., Vincent, F., Volpe, B., Guidetti, R., Harris, N., Beck, A., and Boero, G.: NMR spectroscopy of single sub-nL ova with inductive ultra-compact single-chip probes, Scientific Reports, 7, 10.1038/srep44670, 2017.

380 H. Bürkle, T. Klotz, R. Krapf, and Anders, J.: A 0.1 MHz to 200 MHz high-voltage CMOS transceiver for portable NMR systems with a maximum output current of 2.0 App, IEEE 47th European Solid State Circuits Conference, Grenoble, France, 13-22 Sept. 2021, 10.1109/ESSCIRC53450.2021.9567823, 2021.

H. Bürkle, K. Schmid, T. Klotz, R. Krapf, and Anders, J.: A high voltage CMOS transceiver for low-field NMR with a maximum output current of 1.4 App, 2020 IEEE International Symposium on Circuits and Systems Sevilla, Spain,

385 10.1109/ISCAS45731.2020.9181025, 2020.

Ha, D., Paulsen, J., Sun, N., Song, Y. Q., and Ham, D.: Scalable NMR spectroscopy with semiconductor chips, Proceedings of the National Academy of Sciences of the United States of America, 111, 11955-11960, https://doi.org/10.1073/pnas.1402015111, 2014.

Handwerker, J., Eder, M., Tibiletti, M., Rasche, V., Scheffler, K., Becker, J., Ortmanns, M., and Anders, J.: An Array of Fully-Integrated Quadrature TX/RX NMR Field Probes for MRI Trajectory Mapping, Proc Eur Solid-State, 217-220, 10.1109/ESSCIRC.2016.7598281, 2016.

Handwerker, J., Ortmanns, M., Anders, J., Eschelbach, M., Chang, P., Henning, A., Scheffler, K., and Ieee: An Active TX/RX NMR Probe for Real-Time Monitoring of MRI Field Imperfections, 2013 Ieee Biomedical Circuits and Systems Conference, Rotterdam, Netherlands, 10.1109/BioCAS.2013.6679672, 2013.

Handwerker, J., Perez-Rodas, M., Beyerlein, M., Vincent, F., Beck, A., Freytag, N., Yu, X., Pohmann, R., Anders, J., and Scheffler, K.: A CMOS NMR needle for probing brain physiology with high spatial and temporal resolution, Nature Methods, 17, 64–67, 10.1038/s41592-019-0640-3, 2020.

Hong, S. J. and Sun, N.: Portable CMOS NMR System With 50-kHz IF, 10-mu s Dead Time, and Frequency Tracking, Ieee Transactions on Circuits and Systems I-Regular Papers, 68, 4576-4588, 10.1109/Tcsi.2021.3107286, 2021.

Hoult, D. I.: The principle of reciprocity in signal strength calculations - A mathematical guide, Concepts in Magnetic Resonance, 12, 173-187, https://doi.org/10.1002/1099-0534(2000)12:4<173::AID-CMR1>3.0.CO;2-Q, 2000.

Hoult, D. I. and Richards, R. E.: SIGNAL-TO-NOISE RATIO OF NUCLEAR MAGNETIC-RESONANCE EXPERIMENT, J Magn Reson, 24, 71-85, https://doi.org/10.1016/0022-2364(76)90233-x, 1976.

Issadore, D., Min, C., Liong, M., Chung, J., Weissleder, R., and Lee, H.: Miniature magnetic resonance system for point-of-care diagnostics, Lab on a chip, 11, 2282-2287, 10.1039/c1lc20177h, 2011.

J. Anders, SanGiorgio, P., and Boero, G.: A quadrature receiver for µNMR applications in 0.13µm CMOS, 2010 Proceedings of ESSCIRC, Seville, Spain, 10.1109/ESSCIRC.2010.5619726, 2010.

Keeler, J.: Understanding NMR Spectroscopy, WILEY-VCH2013.

Kim, J., Hammer, B., and Harjani, R.: A Low Power CMOS Receiver for a Tissue Monitoring NMR Spectrometer, Symp Vlsi Circuits, 221-222, 10.1109/Vlsic.2010.5560291, 2010.

Kim, J., Hammer, B., and Harjani, R.: A 5-300MHz CMOS Transceiver for Multi-Nuclear NMR Spectroscopy, 2012 Ieee Custom Integrated Circuits Conference WOS:000310365600071, 10.1109/CICC.2012.6330645, 2012.

Lee, H., Sun, E., Ham, D., and Weissleder, R.: Chip-NMR biosensor for detection and molecular analysis of cells, Nature medicine, 14, 869-874, 10.1038/nm.1711, 2008.

Lei, K.-M., Mak, P.-I., Law, M.-K., and Martins, R. P.: A palm-size mu NMR relaxometer using a digital microfluidic device and a semiconductor transceiver for chemical/biological diagnosis, Analyst, 140, 5129-5137, 10.1039/c5an00500k, 2015.

Lei, K. M., Mak, P. I., Law, M. K., and Martins, R. P.: A mu NMR CMOS Transceiver Using a Butterfly-Coil Input for Integration With a Digital Microfluidic Device Inside a Portable Magnet, Ieee Journal of Solid-State Circuits, 51, 2274-2286, 10.1109/jssc.2016.2579158, 2016a.

Lei, K. M., Heidari, H., Mak, P. I., Law, M. K., Maloberti, F., and Martins, R. P.: A Handheld 50pM-Sensitivity Micro-NMR CMOS Platform with B-Field Stabilization for Multi-Type Biological/Chemical Assays, Isscc Dig Tech Pap I, San Francisco, CA, USA, WOS:000382151400197, 10.1109/ISSCC.2016.7418113, 2016b.

Lei, K. M., Heidari, H., Mak, P. I., Law, M. K., Maloberti, F., and Martins, R. P.: A Handheld High-Sensitivity Micro-NMR CMOS Platform With B-Field Stabilization for Multi-Type Biological/Chemical Assays, Ieee Journal of Solid-State Circuits, 52, 284-297, 10.1109/jssc.2016.2591551, 2017.

Lei, K. M., Ha, D., Song, Y. Q., Westervelt, R. M., Martins, R., Mak, P. I., and Ham, D.: Portable NMR with Parallelism, Analytical Chemistry, 92, 2112-2120, 10.1021/acs.analchem.9b04633, 2020.

Liong, M., Hoang, A. N., Chung, J., Gural, N., Ford, C. B., Min, C., Shah, R. R., Ahmad, R., Fernandez-Suarez, M., Fortune, S. M., Toner, M., Lee, H., and Weissleder, R.: Magnetic barcode assay for genetic detection of pathogens, Nature communications,
430   4, 10.1038/ncomms2745, 2013.

Liu, Y., Sun, N., Lee, H., Weissleder, R., and Ham, D.: CMOS mini nuclear magnetic resonance system and its application for biomolecular sensing, 2008 IEEE International Solid-State Circuits Conference 140-602, 10.1109/ISSCC.2008.4523096,

Minard, K. R. and Wind, R. A.: Solenoidal microcoil design - Part II: Optimizing winding parameters for maximum signal-to-noise performance, Concepts in Magnetic Resonance, 13, 190-210, 10.1002/cmr.1008, 2001.

435   Morris, G. A., Barjat, H., and Horne, T. J.: Reference deconvolution methods, Progress in Nuclear Magnetic Resonance Spectroscopy, 31, 197-257, 10.1016/S0079-6565(97)00011-3, 1997.

Peng, W. K., Kong, T. F., Ng, C. S., Chen, L., Huang, Y. X., Bhagat, A. A. S., Nguyen, N. T., Preiser, P. R., and Han, J.: Micromagnetic resonance relaxometry for rapid label-free malaria diagnosis, Nature medicine, 20, 1069-1073, 10.1038/nm.3622, 2014.

440   Rahman, A.-u., Choudhary, M. I., and Wahab, A.-t.: Creating NMR Signals, in: Solving problems with NMR spectroscopy, Academic Press,, 35-98, https://doi.org/10.1016/B978-0-12-411589-7.00002-4, 2016.

Rudszuck, T., Nirschl, H., and Guthausen, G.: Perspectives in process analytics using low field NMR, J Magn Reson, 323, 10.1016/j.jmr.2020.106897, 2021.

Singh, K. and Blumich, B.: Compact low-field NMR spectroscopy and chemometrics: A tool box for quality control of raw rubber,
445   Polymer, 141, 154-165, 10.1016/j.polymer.2018.02.057, 2018.

Solmaz, N. S., Grisi, M., Matheoud, A. V., Gualco, G., and Boero, G.: Single-Chip Dynamic Nuclear Polarization Microsystem, Analytical Chemistry, 92, 9782-9789, 10.1021/acs.analchem.0c01221, 2020.

Stapf, S. H. S.-I.: NMR imaging in chemical engineering, WILEY-VCH2010.

Sun, N., Liu, Y., Lee, H., Weissleder, R., and Ham, D.: CMOS RF biosensor utilizing nuclear magnetic resonance, IEEE Journal
450   of Solid-State Circuits, 44, 1629-1643, 10.1109/JSSC.2009.2017007, 2009.

Sun, N., Yoon, T.-J., Lee, H., Andress, W., Weissleder, R., and Ham, D.: Palm NMR and 1-chip NMR, IEEE Journal of Solid-State Circuits, 46, 342-352, 10.1109/JSSC.2010.2074630, 2011.

Wu, N. A., Peck, T. L., Webb, A. G., Magin, R. L., and Sweedler, J. V.: H-1-NMR SPECTROSCOPY ON THE NANOLITER SCALE FOR STATIC AND ONLINE MEASUREMENTS, Analytical Chemistry, 66, 3849-3857, 10.1021/ac00094a003, 1994.

455   Wu, Z. X., Lu, R. S., Jiang, X. W., Wang, J. N., Chen, Y., Feng, P., Xie, Z. H., Ni, Z. H., Yi, H., and Xiao, D.: An NMR Relaxation Method of Characterizing Hydrogen-Bearing Crystalline Solid Phases in Hydrated Cement Paste, Ieee T Instrum Meas, 10.1109/TIM.2021.3137163, 2021.

Yang, Q., Wang, J. N., Hu, Z., Ni, Z. H., Lu, R. S., and Yi, H.: A low-cost, miniature Halbach magnet designed for portable time domain NMR, Int. J. Appl. Electromagn. Mech., 65, 59-73, 10.3233/Jae-200001, 2021.

460   Yu, P., Xu, Y. J., Wu, Z. Y., Chang, Y., Chen, Q. Y., and Yang, X. D.: A low-cost home-built NMR using Halbach magnet, J Magn Reson, 294, 162-168, 10.1016/j.jmr.2018.07.014, 2018.